

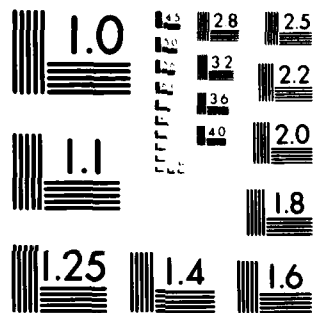
BOSTON COLL CHESTNUT HILL MA SPACE DATA ANALYSIS LAB F/6 17/7
SIGNAL DETECTION/ANALYSIS OF IONOSPHERIC AND GROUNDWAVE PROPAGA--ETC(U)
APR 78 W C MCCOMISH F19628-76-C-0006
BC-SDAL-78-1 RADC-TR-78-198 NL

UNCLASSIFIED

RADC-TR-78-198

NL

END
DATE
FILMED
7 80
DTIC



MICROCOPY RESOLUTION TEST CHART
NATIONAL BUREAU OF STANDARDS-1963-A

78-198

ADA 085757

Approved for public release; distribution unlimited.

DTIC
ELECTE
JUN 13 1980

HOME AIR DEVELOPMENT CENTER
AIR FORCE SYSTEMS COMMAND
GRIFFISS AIR FORCE BASE, NEW YORK 13441

80 6 12 108

FOR THE COMMISSIONER

PLANT OFFICE

UNCLASSIFIED

SECURITY CLASSIFICATION OF THIS PAGE (When Data Entered)

19 REPORT DOCUMENTATION PAGE		READ INSTRUCTIONS BEFORE COMPLETING FORM	
1. REPORT NUMBER (18) RADC/TR-78-198	2. GOVT ACCESSION NO. ✓ AD-A085 757	3. RECIPIENT'S CATALOG NUMBER	
4. TITLE (and Subtitle) (6) SIGNAL DETECTION/ANALYSIS OF IONOSPHERIC AND GROUNDWAVE PROPAGATION	5. TYPE OF REPORT & PERIOD COVERED (9) Final Report 1 Jul 75 - 30 Sep 77	6. PERFORMING ORG. REPORT NUMBER (14) BC-SDAL-78-1	
7. AUTHOR(s) (10) William C. McComish	8. CONTRACT OR GRANT NUMBER(s) (15) F19628-76-C-0006	9. PROGRAM ELEMENT, PROJECT, TASK AREA & WORK UNIT NUMBERS (16) 61102F 2305J221 (17) J2	
10. PERFORMING ORGANIZATION NAME AND ADDRESS Trustees of Boston College ✓ Chestnut Hill, Massachusetts 02167	11. CONTROLLING OFFICE NAME AND ADDRESS (11) Deputy for Electronic Technology (RADC) Hanscom AFB, Massachusetts 01731 Monitor/Gary S. Sales/EEP	12. REPORT DATE 1 Apr 78	
13. MONITORING AGENCY NAME & ADDRESS (if different from Controlling Office) (12) 466	14. SECURITY CLASS. (of this report) Unclassified	15. DECLASSIFICATION/DOWNGRADING SCHEDULE	
16. DISTRIBUTION STATEMENT (of this Report) Approved for public release; distribution unlimited.			
17. DISTRIBUTION STATEMENT (of the abstract entered in Block 20, if different from Report)			
18. SUPPLEMENTARY NOTES			
19. KEY WORDS (Continue on reverse side if necessary and identify by block number)			
Signal Detection Kalman Filtering Grid Prediction Groundwave Propagation Maximum Entropy Estimator Polar Fox II Backscatter-Sea, Ionogram Radar Refraction Doppler Arrival Angle			
20. ABSTRACT (Continue on reverse side if necessary and identify by block number)			
A treatise on the theory and application of various types of analysis and data processing for both ionospheric HF signal propagation and groundwave LF propagation.			

DD FORM 1 JAN 73 1473

EDITION OF 1 NOV 65 IS OBSOLETE

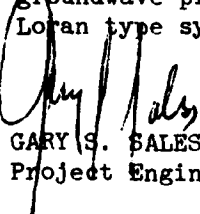
UNCLASSIFIED

403460

SECURITY CLASSIFICATION OF THIS PAGE (When Data Entered)

EVALUATION

1. This evaluation covers the final report on the subject contract by Boston College. This report describes the theory and application of several methods of signal analysis and data processing for both ionospheric HF propagation and groundwave LF propagation.
2. The objective of this work was to develop advanced signal processing techniques that would improve the target detectability of an AF radar in a realistic environment. Several methods were to be compared. In the low frequency part of the spectrum the analysis was aimed at describing the propagation of radio waves over an irregular, finite conducting ground.
3. The results of the radar signal processing analysis are important although they are relatively negative in character. That is, the advanced methods seem to produce no significant improvement over the more conventional analysis. This conclusion will not necessarily be true of all types of data. The effort described in this report on the low frequency groundwave propagation was a major contribution to an operational tool for Loran type systems.


GARY S. SALES
Project Engineer

Dist.		Special
A		

PREFACE

Dr. Gary S. Sales, RADC/EEP, in addition to being the Contract Monitor on Sections 2 and 3, has been the guiding force behind this effort.

Samuel Horowitz, RADC/EEP, was the Contract Monitor on Section 4 and designed the overall program architecture as well as providing the critical interface with previous contracting agencies.

Robert F. Boudreau of Boston College performed the initial sea backscatter data analysis of Section 2, and the software integration in Section 4.

Paul Connolly of Boston College performed the Kalman filtering analysis of Section 4 under the direction of Dr. Terrence Elkins.

Kenneth Dieter of Boston College performed the analysis and data processing of Section 5.

Dr. Rajan Varad* wrote the MEM account in Appendix A.

*formerly of Boston College, presently at Lincoln Laboratory.

TABLE OF CONTENTS

<u>Section</u>	<u>Page</u>
PREFACE	v
LIST OF ILLUSTRATIONS	viii
1 INTRODUCTION	1
2 MAXIMUM ENTROPY ESTIMATOR	1
2.1 Analytical Background	1
2.2 Application to DAASM Data	3
2.3 Application to Sea Backscatter Data	3
2.4 Results & Conclusions	5
3 HF IONOSPHERIC PROPAGATION - POLAR FOX II	6
3.1 Data Processing & Mode Identification	6
3.2 Backscatter Reflectivity Model	7
4 LF GROUNDWAVE PROPAGATION	8
4.1 System Description (LORAN-D)	8
4.2 Terrain Electrical Characteristics	9
4.3 Time Difference Grid Prediction	10
4.4 Results	12
5 RADAR REFRACTION USING VERTICAL-INCIDENCE IONOGRAMS	13
APPENDIX A	15
APPENDIX B	19

LIST OF ILLUSTRATIONS

<u>Figure</u>		<u>Page</u>
1	DAASM 142-2, 2 Pole MEM vs. FFT	20
2	DAASM 142-2, 4 Pole MEM vs. FFT	21
3	DAASM 142-2, 16 Pt. Time Series and 256 Frequencies, DFT	22
4	DAASM 142-4, 4 Pole MEM vs. FFT	23
5	DAASM 142-4, 7 Pole Mem vs. FFT	24
6	DAASM 142-4, 16 Pt. Time Series and 256 Frequencies, DFT	25
7	Sea Scatter, 128 Pt. Time Series (Hanning Window) 512 Frequency, FFT	26
8	Sea Scatter, 128 Pt. Time Series (No Hanning) 512 Frequency FFT	27
9	Sea Scatter, 128 Pt. Time Series, 16 Pole MEM 512 Frequency DFT	28
10	Sea Scatter, 128 Pt. Time Series, 32 Pole MEM 512 Frequency DFT	29
11	Sea Scatter, 128 Pt. Time Series, 64 Pole MEM 512 Frequency DFT	30
12	Sea Scatter, 32 Pt. Time Series, 16 Pole MEM 128 Frequency DFT	31
13	Polar Fox II Coverage	32
14a	Signal Frequency vs. Range Ionogram	33
b	Doppler Frequency vs. Range B/S	
15	Three Dimensional Plot, Doppler vs. Range vs. Power	34
16	Types of Backscatter (B/S)	35
17	Effective Vertical Angle	36
18	LORAN Navigation Hyperbolic Grid Radio Fix	37

1. INTRODUCTION

This final report discusses the theory and application of various types of analysis and data processing for both ionospheric HF signal propagation and groundwave LF propagation.

Much of the analysis pertaining to power spectra and coherence has been dealt with in previous reports [2]. The results of applying the Maximum Likelihood Method to aircraft signal data has been detailed in [3],[16],[17]. The main effort of this report will deal with the Maximum Entropy Estimator Method, its derivation and application to data from the Doppler Arrival Angle Spectral Measurements (DAASM) program and to the sea backscatter measurements from the Ava-Dexter HF radar facility of Rome Air Development Center.

Effort was also directed to the complimentary task of decoding, display, and analysis of A.R.P.A. Polar Fox II ionospheric backscatter data, representing Doppler spectra vs. range.

The LORAN grid prediction program called HUFLOC was a distinct problem that sought to combine groundwave propagation theory with a suitable model for terrain and soil electrical characteristics in order to derive an adaptive estimate of time of arrival differences for various signals used in the LORAN-D navigation system.

An extensive effort was made in Section 5 to extract the most information regarding radar refraction and electron density profiles from a survey of vertical incidence ionograms, using existing techniques and programs.

2. MAXIMUM ENTROPY ESTIMATOR

2.1 Analytical Background

This study is intended to evaluate the performance of the Fast Fourier Transform vs. the Maximum Entropy Method estimate in the processing of short data sequences in an OTH radar environment. Frequently, a radar is designed to operate using spectra estimated from samples whose duration corresponds to minimum coherency intervals. Several such short spectra are averaged before decisions are made concerning the presence or absence of target signals. The preference for the frequency-domain as the starting point of

analysis is dictated by the presence of strong ground clutter returns in a frequency band around DC. The target signals will be well separated from this clutter signal because of the Doppler frequency shift due to the motions of the target. Since the question of determining the maximum sample size for evaluation of spectra depends crucially on the coherence times and scan-mode of the radar, a typical specification for the operational mode of the radar and the ionospheric environment which effects coherence times is assumed.

Once the time samples are transformed into the frequency domain, vectorial addition of corresponding Doppler Fourier spectra from successive blocks proves futile if block size is too small. Incoherent averaging or scalar addition of corresponding power spectra is the only method available when small block sizes (short time samples) are employed. However, if higher resolution spectra are calculated from the same temporal sequences appropriately augmented with zeroes, the spectra can then be incoherently added to obtain some expected improvement in signal estimate reliability over the small block average (a discrete Fourier Transform (DFT) that computes more frequency points than that of the time series is equivalent to a FFT of the augmented time series).

Techniques for Signal Processing - Two techniques for signal processing have been employed on data using actual aircraft signals. They are respectively incoherent FFT averaging (Bartlett-Welch) and incoherent maximum entropy spectral averaging. Here FFT stands for Fast Fourier Transform. The different techniques will be briefly outlined in the following paragraphs.

FFT Incoherent Averaging - In the incoherent averaging, a data sample of say 128 complex valued points is broken into 15 overlapping segments of 16 points each and a FFT is performed on each of the 15 blocks or segments. An estimate of the power spectra is made for each of the blocks and an average of the corresponding Doppler power spectra over the blocks is computed. Since no phase information is utilized in computing the average the method is called incoherent averaging.

MEM Incoherent Averaging - The second technique is similar to the first one except that the power spectrum for each block is calculated by using the maximum entropy method (MEM). The MEM is well known and has been described

by Burg (4), Lacoss (1), and Smylie et al. (5). Varad (2) has independently developed and applied the MEM algorithm to evaluate power, coherence and phase spectra where the input samples are complex valued multi-channel data points. Superior spectral resolution using MEM estimates, particularly for short data samples, was expected. The MEM involves recursive estimation of Anderson coefficients (5). The MEM spectra are averaged in the same manner as the incoherent averaging technique. The mathematical details for these techniques are presented in Appendix A.

2.2 Applications to DAASM Data [16],[17]

Aircraft target data from the DAASM program presents a signal displaced from the ground clutter, except for velocities corresponding to the Nyquist frequency, ± 4 Hz. The basic Doppler frequency range is 8 Hz. A data set is comprised of 128 equally spaced complex time samples from each antenna channel and each range gate. No interlacing from the two sets of equally spaced time samples was used in this study, so that Doppler frequencies greater than ± 4 Hz are aliased into the basic Doppler frequency range. The data sample is divided into 15 blocks of 16 points each with a 50% overlap factor to reduce variation from block to block. Figures 1 through 6 present the 16 point incoherent block average of the spectra provided by the MEM with 16 and 256 frequency points calculated, compared with the DFT for 16 and 256 computed frequency points. The MEM was calculated for 2, 4, and 7 filter poles. The FFT has a 3 point Hanning window applied.

2.3 Applications to Sea Backscatter Data

Sea scatter data from RADC Ava-Dexter HF radar was analyzed with both the FFT and complex MEM techniques using a variety of choices for data length.

When reflected from a land mass, the spectra typically peak at zero frequency (no Doppler shift), indicating no local movement in the reflecting area. However, when reflected from an ocean region, the returned signals yield two distinct Doppler peaks the amplitude of which is proportional to the direction of local ocean wave movement in the reflecting area. Other objects moving through the reflecting area, such as ships or airplanes, can also be detected as lower level peaks within or near the same Doppler range as the sea clutter.

Because the spectral band of interest extends only over a small area of the lower frequencies, fine resolution is required in the frequency domain to readily observe the two Doppler peaks and the frequency band between them. Typically, very long time samples of radar backscatter have been recorded and processed to the spectral domain by conventional Fourier analysis. Under these conditions, the Doppler peaks are resolved directly as a function of the length of the time samples [15]. Theoretically, the same spectral data resolution should be able to be obtained from shorter time samples, where spectral analysis would be performed by the recently developed Complex Maximum Entropy Method.

The purpose of this effort then is to verify existence of certain Doppler signals, obtained from conventional Fourier analysis of long time data samples read from magnetic tape recordings of ocean radar backscatter. Having shown the resolving power of this method, relative to data length, a comparative spectral resolution analysis by Complex MEM should theoretically then determine some minimum data length which can realistically be generally applied to signal detection from radar backscatter information.

Analytical/Programmable Effort - Computer programs have been written to read given magnetic tape recordings of time domain radar backscatter data. For initial observation of power spectra behavior, computational programs were written, and different data sample lengths were analyzed by use of Fast Fourier Transforms acting on the raw time domain data. Initial analysis of the power spectra showed that more detailed information would be desirable.

As the radar information extends over 64 different range bins, one could choose between processing by the so-called Infinite Fast Fourier Transform the entire 64 range samples each with very long data lengths, or stripping information by range and then processing time sequences for the selected ranges. The former required large computer core and processing time, thereby reducing computer turnaround time; the latter required writing additional data handling programs with intermediate disk storage of information. As it was felt that the Complex MEM analysis would probably not be necessary over all 64 ranges, the second option was undertaken.

A program was written from which disk files of time domain information were generated to allow selection of specific ranges by the main analytical routine. For increased spectral resolution, an FFT was applied to the zero-augmented time series with a cosine squared window (Hanning filter) imposed only on the basic input time interval. [Bartlett-Welch block averaging was applied to sequences of computed power spectra to improve overall signal estimation reliability.] The resulting power spectra are displayed in Figures 7 and 8.

2.4 Results & Conclusions

The new MEM routine produced reasonable and consistent Bragg line spectra (Figs. 9-12). Power spectra from the FFT were almost identical, indicating that the natural line width was being displayed at least for a time series of 128 points or more.

The anticipated order of magnitude of Signal-to-Noise improvement was not observed when comparing properly windowed Fourier spectra to optimal MEM spectra. Here, optimal is used in the sense that some optimum number of filter poles was utilized to produce a spectrum of minimum noise and minimum smoothing. While some MEM spectra, produced with larger numbers of filter poles, appear to have more sharpness in spectral peaks, the same sharpness is apparent in the noise level. Overall frequency resolution was comparable when comparing spectra generated from input of the same data lengths. MEM analysis of shorter data lengths did not produce significantly observable spectral peaks in the target areas. Overall, target detectability, small signal detection in the higher Doppler frequency ranges, was not very much different between the Fourier and MEM spectra.

One conclusion to be drawn from this investigation is that it seems certain classes of data are not of a nature as to allow spectral analysis methods based upon prediction-error filters to fully optimize data-adaptive features. The nature of such information is not defined within the context of this study. A possible area of investigation might be system bandwidth characteristics.

Similarly for the DAASM aircraft data, the MEM with a 256 point DFT offers only slight improvement in resolution over the equivalent 256 point FFT of the zero-augmented 16 point time series; compare Figures 4 and 6 or Figures

2 and 3. In general, the number of spectral peaks produced equals the number of MEM filter poles.

3. HF IONOSPHERIC PROPAGATION

3.1 Data Processing & Mode Identification

The Polar Fox II program of the Defense Advanced Research Projects Agency (ARPA) studied ionospheric backscatter signals over the 6 to 26 MHz frequency range in the northern latitudes, with the receiver and transmitter located at Caribou, Maine and scanning azimuths from -30° T to $+60^{\circ}$ T during 1972. The magnetic tapes generated contain two types of data; a fixed frequency, azimuth scanning mode and a fixed azimuth, frequency scanning mode. The frequency scanning mode produced ionograms (frequency vs. range) at 3 fixed azimuths, while the azimuth scanning mode gave a 32 point Doppler spectra at 230 range bins (from 624 km to 4074 km) at 3 discrete frequencies. Figure 13 shows the range coverage and geography of the experiment and Figure 14a presents the digicoder display generated from unpacking and decoding the frequency scanned ionogram data. Reports from the Raytheon Co. and Lincoln Laboratories were the sources for the program developed.

The fixed frequency backscatter (B/S) data was decoded, unpacked and calibrated from the appropriate hourly calibration signal; a noise level determination is available for every minute (i.e., every azimuth) of the 34 minute data interval and this is used as a threshold for displaying the return Doppler signal. Four types of displays were developed:

1. Received power calibrated in dBw from the reference level and thresholded at 6 dB above the 4th decile of noise, 32 Doppler bins per every 3rd range bin, one display for each azimuth beam position. (Figure 14b)
2. A "contour" plot of this display with a different letter assigned to every 10 dB step.
3. A listing line plot of amplitude vs. range bin for the 0, ± 8 and 16 Hz Doppler lines.
4. A three dimensional plot of Doppler vs. range vs. power amplitude for any selected azimuth or frequency. (Figure 15).

Together these plots facilitate the propagation mode identification with the presence of ground clutter, interference lines, etc. The four transmitter powers recorded indicate both total power and antenna operating mode; the azimuth beam pattern gain and beamwidth are derived from the published system description [19].

3.2 Backscatter Reflectivity Model

The next step is to apply the two basic calculations of volumetric backscatter (VBR) and surface backscatter reflectivity (SBR) to this total received power. The takeoff elevation angle is determined as a geometric function of range; ionospheric absorption as a function of geomagnetic latitude [7], and the assumed elevation orthogonality angle are also needed (Appendix B). The VBR and SBR equations were developed by G. S. Sales [6]. The resulting calculations can be made for ionospheric E and F layer heights and different propagation mode options. (Figures 16 and 17.)

The synoptic data tapes were revived and used to display larger periods of mode identifications; a short program was coded for this purpose. Previous attempts to analyze this data at other facilities has produced results questionable from the point of view of mode identification and which, moreover took no account of antenna sidelobes in the azimuth identification. The continuing analysis effort will attempt to incorporate antenna radiation patterns, at least to the extent of avoiding gross mislocation of the clutter scattering area. This is a definite possibility in view of the poor sidelobe suppression as the antenna is steered to large angles off boresight. An effort must be made to check the internal consistency of the data for clues to sidelobe or backlobe reception as well as reasonable agreement with nominal reflectivity values for standard types of clutter. Also, samples of data recorded at times and frequencies differing by a small amount, showing conflicting mode identification for the same geographical region, will be studied more closely. Clearly, error can result if the received backscatter came from a different direction than that immediately indicated by the antenna bearing, since certain assumptions must be made about the ionosphere in the region from which the backscatter is assumed to originate.

4. LF GROUNDWAVE PROPAGATION

4.1 System Description - LORAN-D

LORAN-D is a hyperbolic system of navigation wherein a radio navigation fix is obtained as the intersection of two hyperbolic lines of position (Fig. 18). These hyperbolic lines are synthesized from a set of three pulse transmitters comprising a master M and two slaves, S_1 and S_2 separated by a convenient baseline length d_{b1} and d_{b2} . The navigator's line of position is expressed as a constant time difference TD where

$$TD = \frac{n_1}{c} (d_b + d_s - d_m) + t_c d_b + t_c d_s - t_c d_m + e_s$$

where n_1 = index of refraction of air

c = velocity of light

d_b = length of baseline, geodetic line from master to slave

d_m = geodetic line from observation point to master transmitter

d_s = geodetic line from an observation point to a slave transmitter

e_s = coding or emission delay (retransmission time of the slave signal)

t_c = phase correction for propagation over a path of length $d = d_m$,
 d_s, d_b secs.

The distances d_s , d_m and d_b are also geodesics to a particular point O along AB or between master M and slaves s_1 and s_2 . Curved lines have been used to note that geodesics are characterized by a continuous azimuth or direction change along the line. Two hyperbolic lines of position TD1 and TD2 determine the point O at their intersections. Given the geographic coordinates of M, S_1 and S_2 , the coordinates of O can be calculated. However, the phase correction expressed in seconds, t_c , must be known for precision determination. The phase correction becomes

$$\phi_c = \frac{wt_c}{10^6} \quad \text{radians}$$

and

$$f = w/2\pi \quad \text{Hertz}$$

This phase is in turn composed of a primary delay due to a homogenous terrain and a secondary delay due to irregularities and inhomogenities in the terrain. The primary phase factor along the geodetic distance is calculated from the Sodano method [11]. The secondary phase factor, in the method of Johler and Hyovalti is calculated from assumed electrical characteristics of the terrain. Sodano's method has been adapted to incremental geodesic steps by Hufford [8],[9],[10].

In the final software package, the overall program called HUFLOC accepts topographical and geological information from the random access data base; applies impedances calculated from this data base to the geodesic signal paths determined from transmitter and receiver coordinates, calculates the time of arrival of each groundwave (combining primary and secondary phase factor), and finally calculates the two required time differences TD1 and TD2. The two basic programs include a means of calculating geodesic distances between transmitter and receiver by Hufford's method, and then proceed to perform the integration of the signal propagation over the geodesic distances to yield the components (amplitude and phase) of the waveform. A combined integral equation and classical electromagnetic technique is used [8],[9], coded in subroutine INEQ2E.

4.2 Terrain Electrical Characteristics

This effort involved the establishment of the random access data base working from a set of terrain elevation, geologic age and soil classification tapes supplied through the Initiator, the LORAN S.P.O. office. A total input of 37 tapes is used to generate a data base grid of 691,200 points containing packed values of elevation and either complex impedance or geology and soil code, located every 30 arc-seconds over a 6° by 8° geographic area.

Each input geology code tape was itself generated in three steps:

1. Conversion from digitized table coordinates to geographic coordinates, corrected for longitude line conversion
2. A SORT-MERGE routine to select and sequence the resulting data
3. A final conversion to the interpolated 30 arc-second grid.

This conversion sequence was developed and coded for use here on the CDC 6600.

The actual complex impedance is derived from the correspondence table of actual conductivities and dielectric constants along with an assumed model of the soil and rock strata; the resulting impedance is overwritten on the fundamental data base as amplitude and phase. Ten bits are allocated to elevation, 9 bits to amplitude and 11 bits to phase produced an amplitude accuracy of ± 2 ohms, phase accuracy of ± 0.001 radians and elevation to ± 7 meters. These allocations were chosen on the basis of the sensitivity of the computed time of arrival of the groundwave and the measurement accuracy of the conductivity maps. The soil strata model chosen can be changed either for geophysical reasons or as a result of the sensitivity and estimation procedures outlined below.

4.3 Time Difference Grid Prediction

The combined HUFLOC-INEQ2E program accesses the random access data base by means of an index generated from input path vector increments along the geodesic from Master-, Slave 1- and Slave 2-to-receiver and proceeds to solve the integral equation for field intensity and phase delay, primary and secondary. A complete description of the program is given in [12].

Next, a least-squares estimate with a Kalman filter was applied for the empirical correction of the soil conductivity model. The specific approach developed was:

- a. The two values for topsoil conductivity that occurred most frequently in the geographical area of interest would be identified.
- b. The random access data base would be created, and the program which computed the transmission time delay would be run to produce calculated values for approximately 50 locations for which measured, airborne data were available.
- c. The variation of transmission time delay due to variation in topsoil conductivity would be computed by changing, in turn, each of the two conductivity values where they occurred in the geographical area of interest and by proceeding with the steps outlined in paragraph b. above.
- d. The differences between the observed and calculated data, the rates of change in transmission time delay due to changes in each conductivity value, estimates of the error in the initially chosen values of conductivity, and estimates of the error in the observations would be input into the Kalman filter program to produce an improved estimate of the values of conductivity.

- e. Using the improved values of conductivity, the steps outlined in paragraph b. above would be repeated, and the new calculated values could be contrasted with the earlier transmission time delay values.

In order to select the two most frequently occurring values of topsoil conductivity, a modified version of the data base creation program was written. This program displayed all the values of topsoil conductivity in a map-like fashion. It was immediately obvious that there were extraneous values of conductivity along the same line of longitude in numerous places in the geographical area. Many of these values were corrected by scanning along the same latitude line and changing those values which differed from that value which occurred immediately before and after. A similar check was performed for the values of bedrock conductivity. After this preliminary work, the two most frequently occurring values of topsoil conductivity were identified. The locations in the random access data base, where these conductivity values occurred, were identified in order to reduce by 70% to 90% the time required to change the data base.

Calculated values of transmission time delay were made for 43 locations for which observed data was also available. Numerical approximations to the partial derivatives of transmission time delay with respect to each value of conductivity were made by varying each value of conductivity +10% and -10%. New data bases were produced, and calculated values of transmission time delay were made. The partial derivatives were approximated by the quotient of the difference in transmission time delays divided by the difference in conductivity values. These calculations involved 160 lengthy computer runs.

The variance associated with each data measurement was

$$\sigma^2 = \sigma_o^2 \left(\frac{1}{\sin \alpha} \right)^2$$

where σ_o^2 is an input quantity and α is an angle formed by the three points, master transmitter, receiver, and slave transmitter. The standard deviation σ_o of the measurements is assumed to be approximately 100 or 200 nanoseconds. The filter program was run several times in order to determine what changes resulted in the estimate of the values of conductivity. The initial values for the state vector of conductivity values and the state covariance matrix were respectively:

$$\begin{pmatrix} .020618 \\ .008439 \end{pmatrix} \text{ and } \begin{pmatrix} 1. \times 10^{-6} & 0 \\ 0 & 1. \times 10^{-6} \end{pmatrix} .$$

Using values of σ_o equal to 200 nanoseconds and 100 nanoseconds, respectively, the following estimates of the state vector resulted:

$$\begin{pmatrix} .017642 \\ .014592 \end{pmatrix} \text{ and } \begin{pmatrix} .011904 \\ .020085 \end{pmatrix} .$$

New data bases were produced for each of the sets of values, and transmission time delays were calculated for six of the 40 locations available. In general, the differences between observed and calculated time delays decreased as compared to the differences obtained using the original data base. The second estimate, as anticipated, resulted in the smallest differences of the original, first changed, and second changed data bases.

4.4 Results

The predicted time difference grid in general was about 200 nanoseconds, (equivalent to a C.E.P. of about 60 meters) different from measured reconnaissance values from aircraft reception at about 1000 ft. altitude and somewhat better on ground reception: the core memory required to run the HUFLOC program is about 137K and the execution time for a typical target is 130 secs.

5. RADAR REFRACTION USING VERTICAL INCIDENCE IONOGRAMS

The data from the Digisonde-128 were stored on 1200 reels of tape. Originally, one day's worth of data was put on one tape; later on, two days worth. The data themselves represent a digital ionogram which covers a frequency range from 0 MHz to about 12 MHz, although this upper limit can be increased to 16 MHz or even higher. On the vertical scale the ionogram has 128 range bins, the first bin corresponding to 60 km.; each successive bin represents 1.5 km. On the horizontal scale the step size is generally .05 MHz for data gathered at the beginning of an hour; and either .10 or .025 MHz otherwise. If we take the 128 range bins and multiply times the 12/.05 (=240) frequency positions we get about 30,000 points (or possible echoes)

for each ionogram. Since we have about 9 ionograms/hour, and the Digisonde works 24 hour/day, it is apparent that the amount of data is considerable. However, it turns out that only about 200 of these points actually represent the traces of the ionogram; everything else is "noise", or unwanted signals. Therefore, by filtering we were able to compress the data from 1200 tapes down to about 10. The actual method of filtering is described in [13].

The compression operation also involves packing the data for each echo into half of one CDC word. The data stored include the number of the frequency, the number of the range bin, the amplitude of the echo, and the total number of echoes at the given frequency. This information requires 28 bits altogether. Thus, the data for two echoes can be stored in one CDC word.

Trace identification involves the determination of certain critical frequencies and heights from the ionograms. The actual description of the techniques involved can be found in [13].

An important application of filtered ionogram data is that of constructing an electron density profile. The programs already exist for this; all it is necessary to do is to select a group of points from the ionogram and feed them into a profile program and get a plot of height versus electron density. The only problem is selecting the points properly. This is discussed in [14] by Cormier and Dieter. Once an electron density profile for an ionogram is calculated, it is of some interest to apply the curve in computing refraction corrections for a radar system. The problem centered around using different curve-fitting routines for different parts of the profile. We employed a spline curve over the lower part of the profile and an exponential curve over the upper part. This latter curve-fit was described in a previous Boston College report by Power and Martine [18].

APPENDIX A

Maximum Entropy Method

In this section, the mathematical derivations will be presented for the different techniques.

1) Incoherent FFT

Let $x_1(t), x_2(t) \dots x_N(t)$ be the N complex time samples, e.g., $N=128$. The N sample points are divided into L blocks of M sample points and a FFT of length M is performed for each of the L blocks. Thus, the FFT is given by

$$X_K(w) = \sum_{n=0}^{M-1} x_n(t) e^{-jwkn},$$

where K is the discrete frequency. The average power in the k^{th} frequency is calculated from

$$S_K(w) = \frac{1}{L} \sum_{l=1}^L |X_K(w)|^2.$$

A Hanning filter could be implemented by replacing $X_K(w)$ with

$$X_K(w) = \frac{1}{4} X_{K-1}^{(w)} + \frac{1}{2} X_K^{(w)} + \frac{1}{4} X_{K+1}^{(w)}.$$

The end points $X_1(w)$ and $X_{M-1}^{(w)}$ are wrapped around for this estimate.

2) Incoherent MEM

The maximum entropy method of spectral evaluation seeks to determine coefficients of a filter whose output would be ideally white noise when the input is the process under consideration. Thus, if $S(w)$ is the power spectrum of the input data and $H(w)$ is the transfer function of the filter, then

$$S(w) |H(w)|^2 = \sigma^2$$

where σ^2 is the variance of the output. The coefficients comprising $H(w)$ for any given order of the filter are chosen so as to minimize σ^2 . For a $(K+1)^{\text{th}}$ order filter

$$H(w) = 1 + a_{K,1} e^{-jw \cdot 1} + a_{K,2} e^{-jw \cdot 2} + \dots a_{K,K} e^{-jwk}$$

$$= 1 + \sum_{k=1}^K a_{K,k} e^{-jwk}$$

so that

$$S(w) = \frac{\sigma_K^2}{|1 + \sum_{k=1}^K a_{K,k} e^{-jwk}|^2}$$

The coefficients $a_{K,k}$ are calculated in a recursive manner beginning with $a_{11}, a_{22} \dots a_{K-1,K-1}$ and σ_K^2 likewise from $\sigma_0^2, \sigma_1^2 \dots \sigma_{K-1}^2$. Initially

$$\sigma_0^2 = P_1$$

is calculated from

$$P_1 = \sum_{i=0}^{N-1} \chi_i \chi_i^*$$

where χ_i^* represents the complex conjugate of χ_i , the i^{th} time sample.

Next, the autocorrelation for zero lag r_0 is set equal to P_1

$$r_0 = P_1$$

Now r_1 , the autocorrelation for unit lag is calculated from the matrix equation

$$\begin{bmatrix} r_0 & r_1 \\ r_1^* & r_0 \end{bmatrix} \begin{bmatrix} 1 \\ a_{11} \end{bmatrix} = \begin{bmatrix} P_2 \\ 0 \end{bmatrix}$$

where

$$P_2 = \sigma_1^2 = \sum_{i=0}^{N-2} \left\{ |\chi_i + a_{11} \chi_{i+1}|^2 + |\chi_i + a_{11}^* \chi_i|^2 \right\}$$

and a_{11} is obtained by minimizing P_2

$$\frac{\partial P_2}{\partial a_{11}} = 0$$

Here P_2 is being evaluated by forward and backward averaging and the corresponding a_{11} is given by

$$a_{11} = -2 \sum_{i=0}^{N-2} \left\{ x_i x_{i+1}^* / \sum (x_i x_i^* + x_{i+1}^* x_{i+1}) \right\}$$

$$\text{and } P_2 = (1 - a_{11} a_{11}^*) P_1$$

The next recursion is written as

$$\begin{bmatrix} \gamma_0 & r_1 & r_2 \\ \gamma_1^* & r_0 & r_1 \\ \gamma_2^* & r_1^* & r_0 \end{bmatrix} \begin{bmatrix} 1 \\ a_{11} \\ 0 \end{bmatrix} + a_{22} \begin{bmatrix} 0 \\ a_{11}^* \\ 1 \end{bmatrix} = \begin{bmatrix} P_2 \\ 0 \\ \Delta_2 \end{bmatrix} + a_{21} \begin{bmatrix} \Delta_2^* \\ 0 \\ P_2 \end{bmatrix}$$

$$= \begin{bmatrix} P_3 \\ 0 \\ 0 \end{bmatrix}$$

P_3 is found in a similar manner as P_2 by minimizing with respect to a_{22} and given by

$$P_3 = (1 - a_{22} a_{22}^*) P_2$$

$$a_{21} = a_{11} + a_{22} a_{11}^*$$

and

$$a_{22} = \frac{-2 \sum_{i=0}^{N-3} \left\{ x_{i+1} + a_{11} x_{i+2} \quad x_{i+2} + a_{11} x_{i+1} \right\}^*}{\sum_{i=0}^{N-3} \left\{ |x_{i+1} + a_{11} x_{i+2}|^2 + |x_{i+2} + a_{11}^* x_{i+1}|^2 \right\}}$$

Further recursions can be similarly performed and the coefficients at the k^{th} step,

$$a_{K1}, a_{K21}, \dots, a_{K, K-1}, a_{K, K}$$

can be calculated and inserted in the equation for the power spectra, and of course

$$\sigma_K^2 = P_{K+1}$$

is also available recursively.

APPENDIX B

Three basic propagation modes are considered, two associated with ionospheric backscatter and the third with ground backscatter (Fig. 16). Permutations of two basic heights, 100 km and 300 km, are used to establish the possible propagation modes and scattering heights. The atmospheric absorption loss term L was calculated from the method developed in [7].

The ground surface reflectivity ρ_o is defined in terms of measured quantities. For volume scattering, the concept of orthogonal scattering with cylindrically shaped irregularities has been introduced. As in the case for a surface reflector, the azimuthal beam width and pulse width define two of the three required dimensions for scattering volume in the ionosphere which contributes to the received power at a specific time delay or range, R . The third dimension, $R(H)$, has been determined using ray-trace techniques in F-region models of the ionosphere and the required orthogonality with the earth's magnetic field for backscatter.

The effective vertical angle, (H) , is shown in Figure 17 and is determined by ray tracing as having a nominal value of 0.5 degrees.

The two intrinsic reflectivities derived by Sales [6] to characterize the scattering medium are the surface reflectivity

$$\rho_o = \frac{(4\pi)^3 R^4 (L^2)^2}{P_T G_T G_R \lambda^2 (\text{AREA})} P_R \quad \text{units of } M^2/M^2$$

and volume reflectivity

$$\sigma_o = \frac{(4\pi)^3 R^4 (L^2)^{2N+1}}{P_T G_T G_R \lambda^2 (\text{VOLUME})} P_R \quad \text{units of } M^2/M^3$$

where the illuminated area = $\tau(R\Phi)$ in M^2 and the illuminated volume = $\tau(R\Phi)$ $[R(H)]$ in M^3 and

τ = pulse width

ϕ = azimuthal beamwidth

\textcircled{H} = effective vertical angle

N = 0, one leg mode

= 1, three leg mode

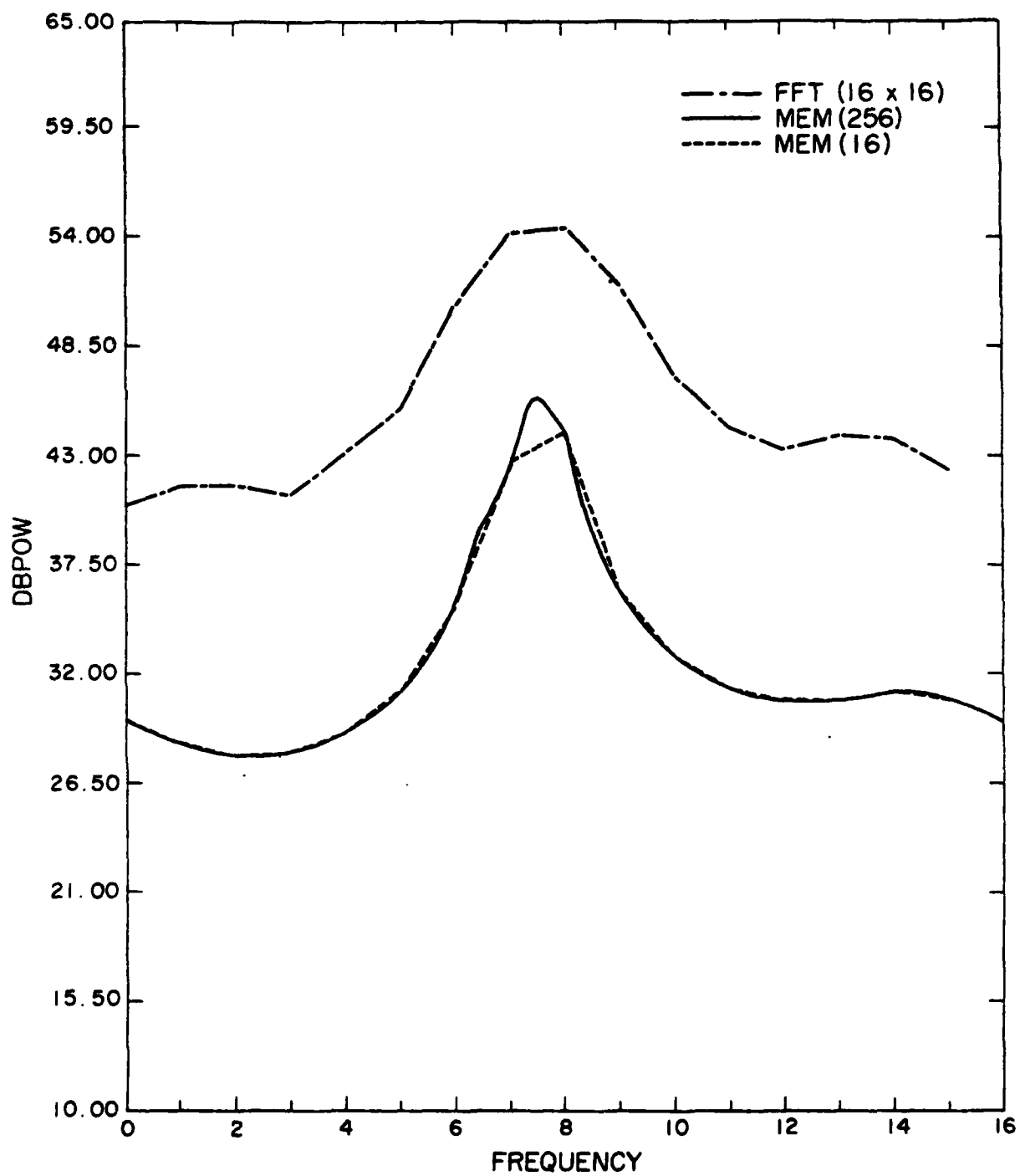


Figure 1. DAASM 142-2, 2 Pole MEM vs. FFT

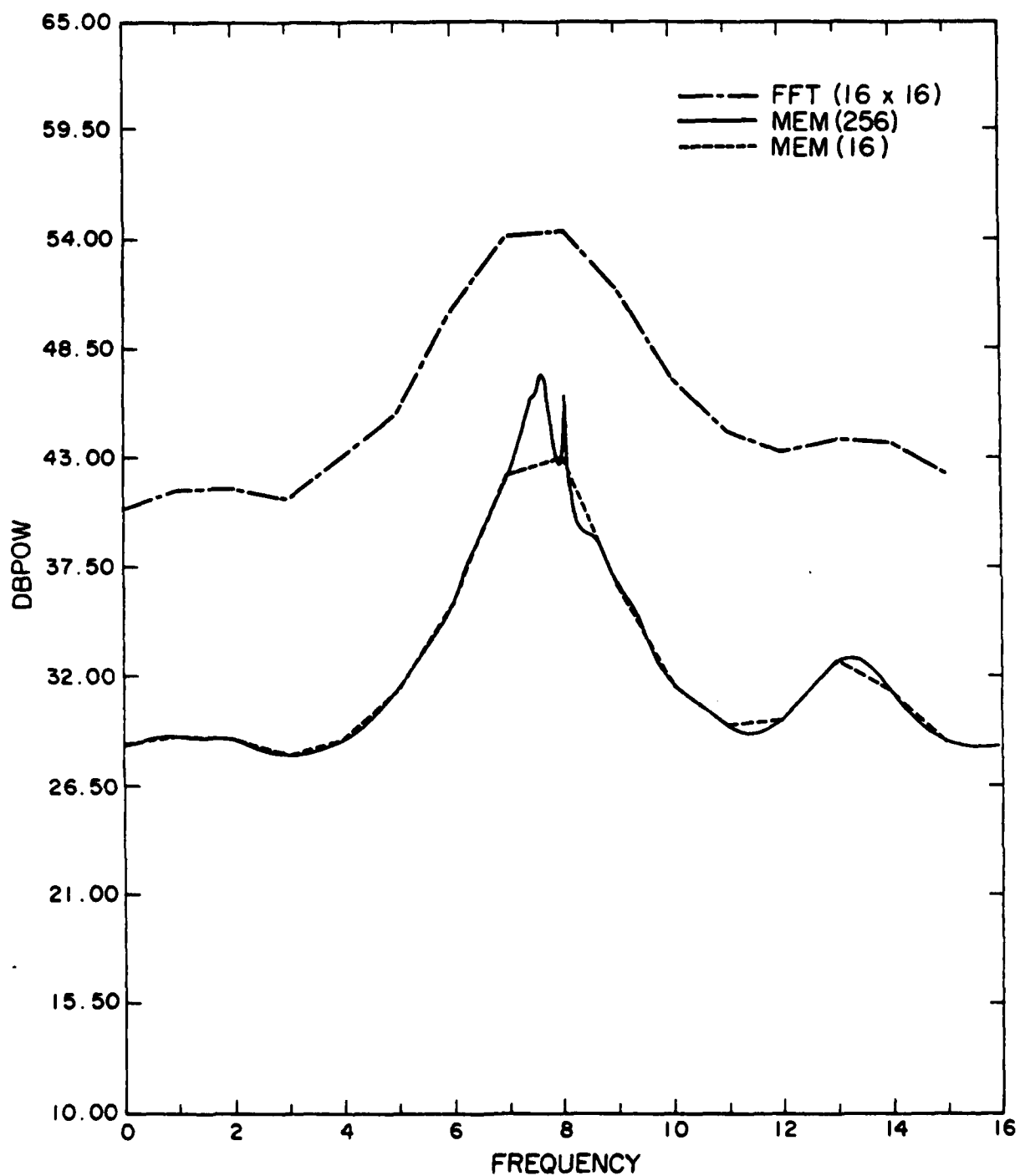


Figure 2. DAASM 142-2, 4 Pole MEM vs. FFT

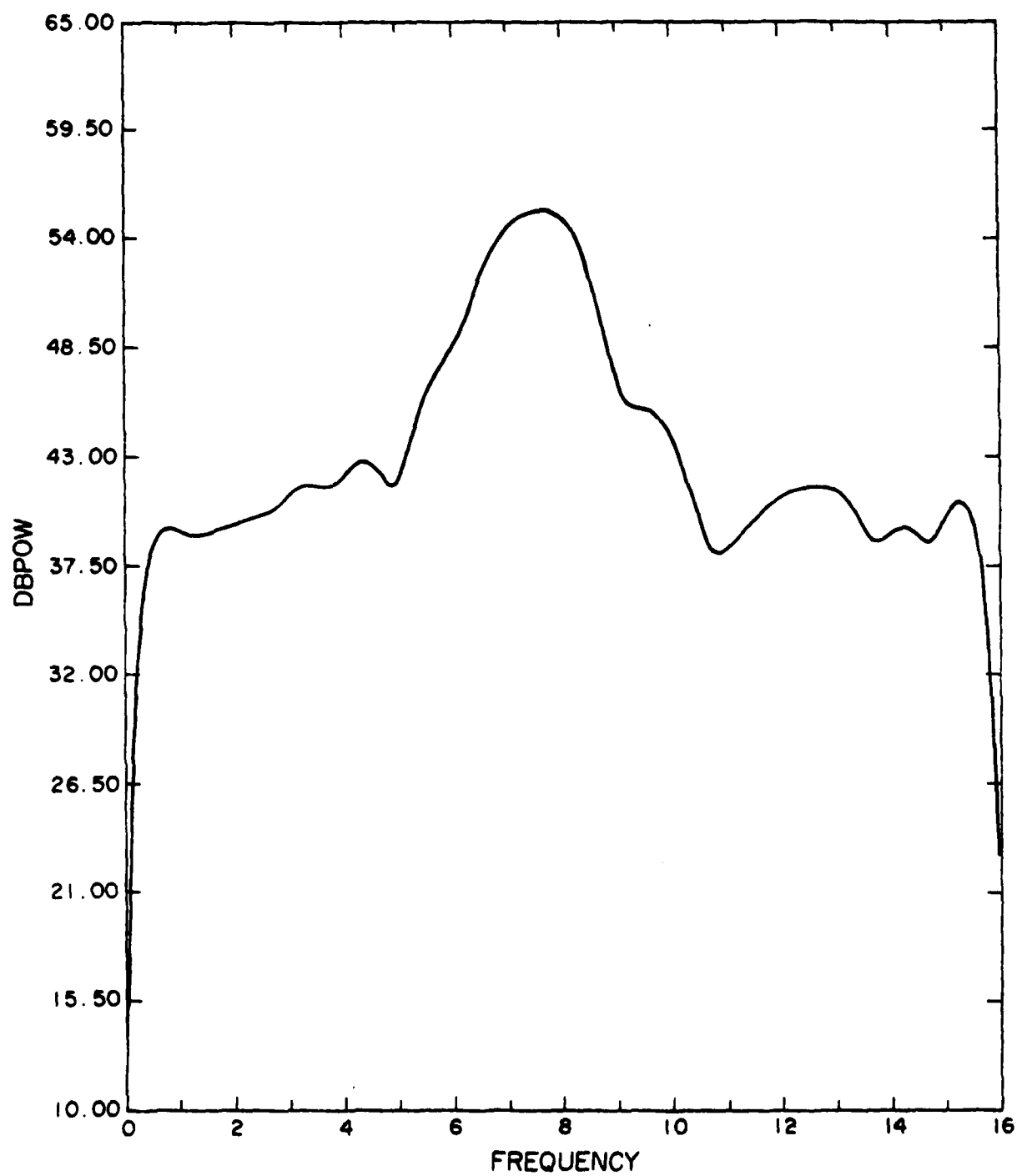


Figure 3. DAASM 142-2, 16 Pt. Time Series and 256
Frequencies, DFT

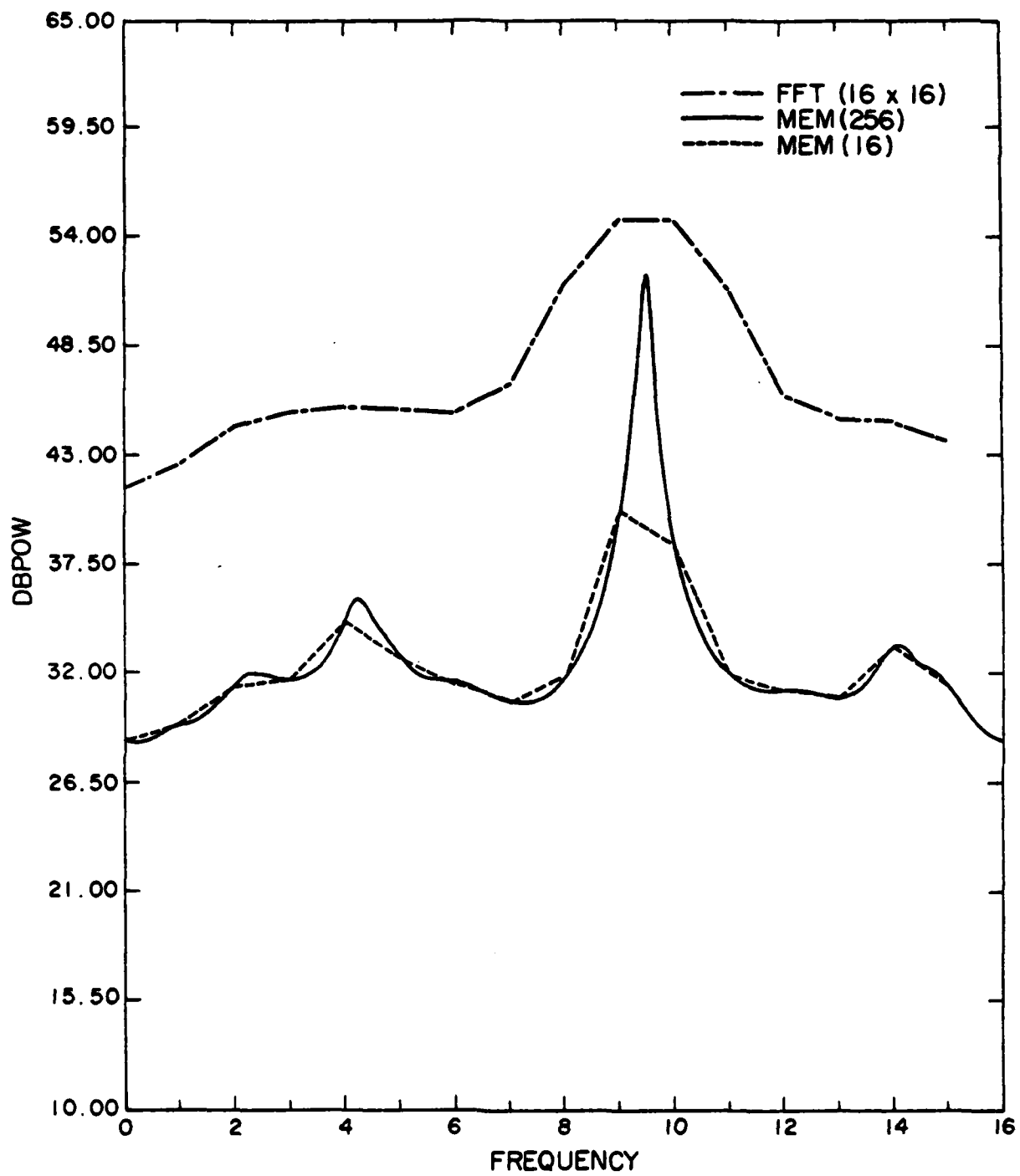


Figure 4. DAASM 142-4, Pole MEM vs. FFT

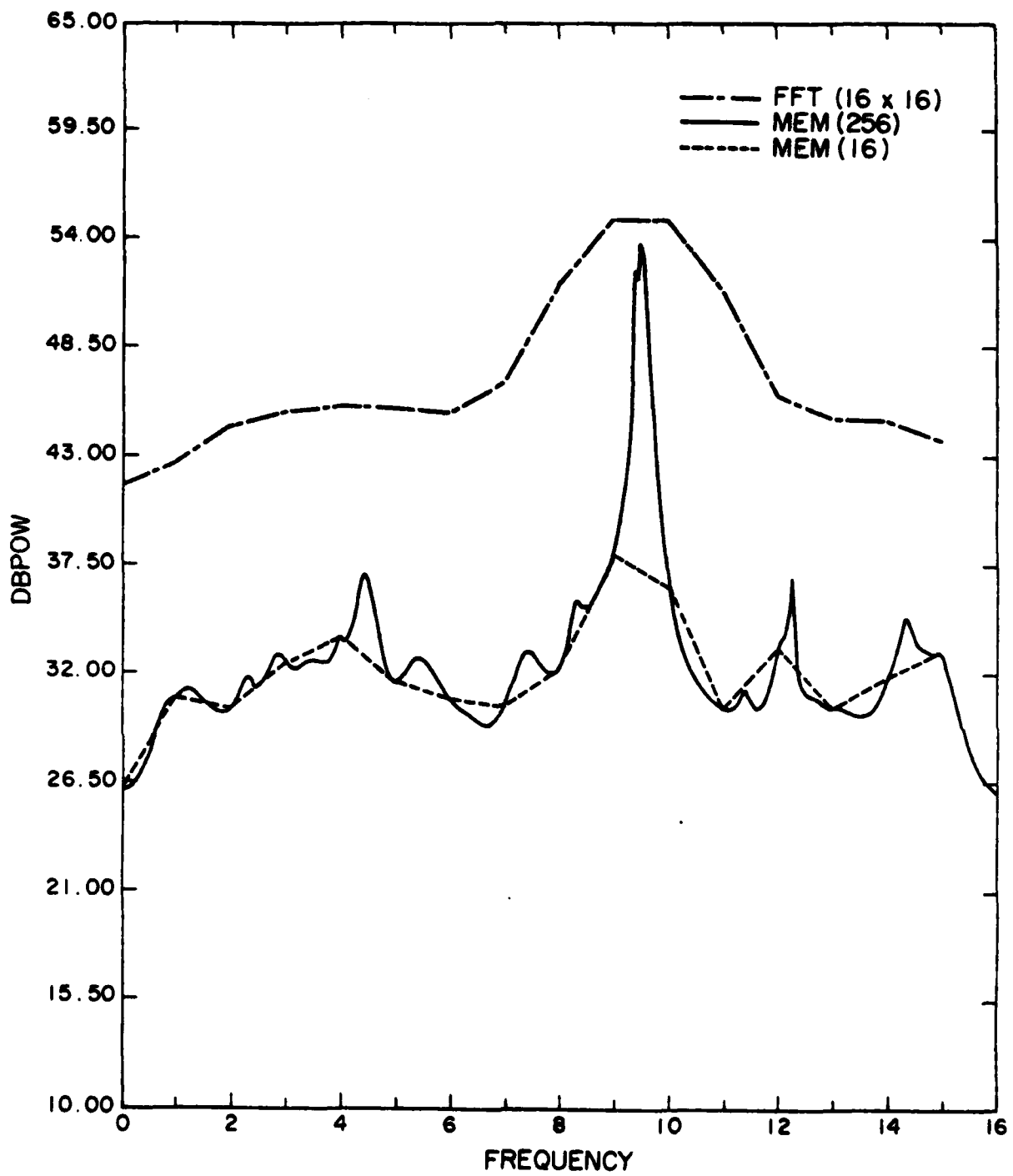


Figure 5. DAASM 142-4, 7 Pole MEM vs. FFT

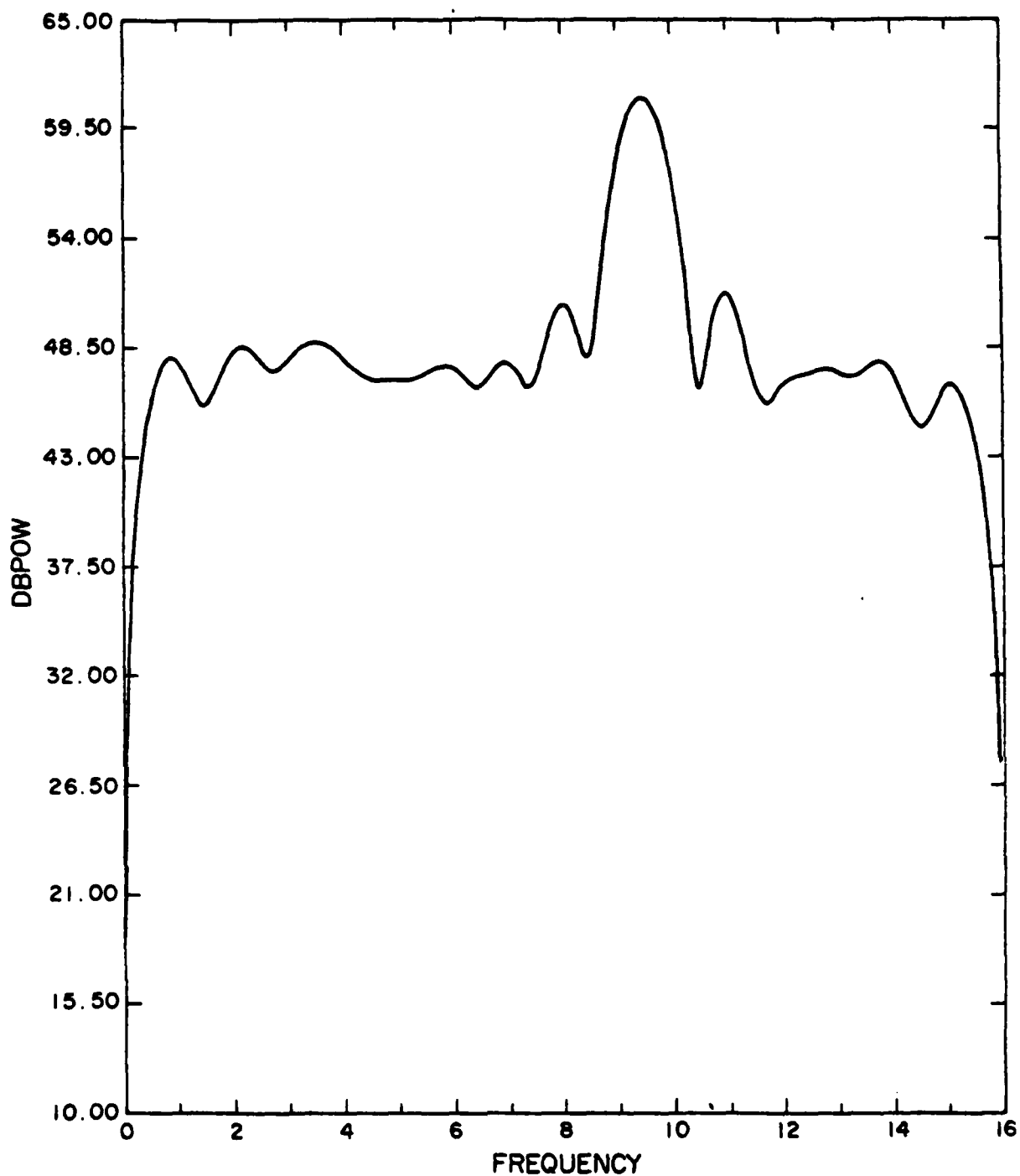


Figure 6. DAASM 142-4, 16 Pt. Time Series and 256
Frequencies, DFT

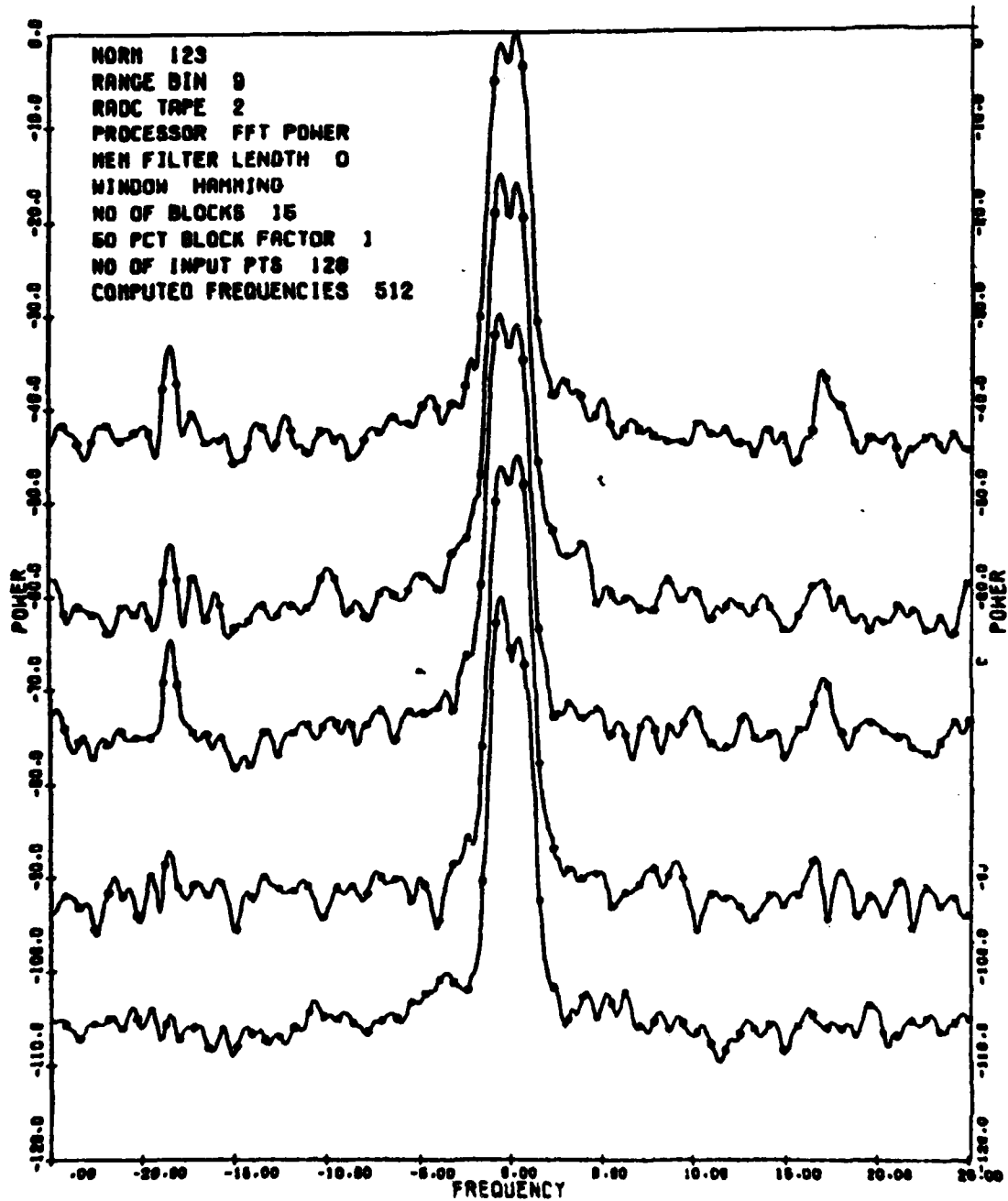


Figure 7. Sea Scatter, 128 Pt. Time Series (Hanning Window) 512 Frequency, FFT

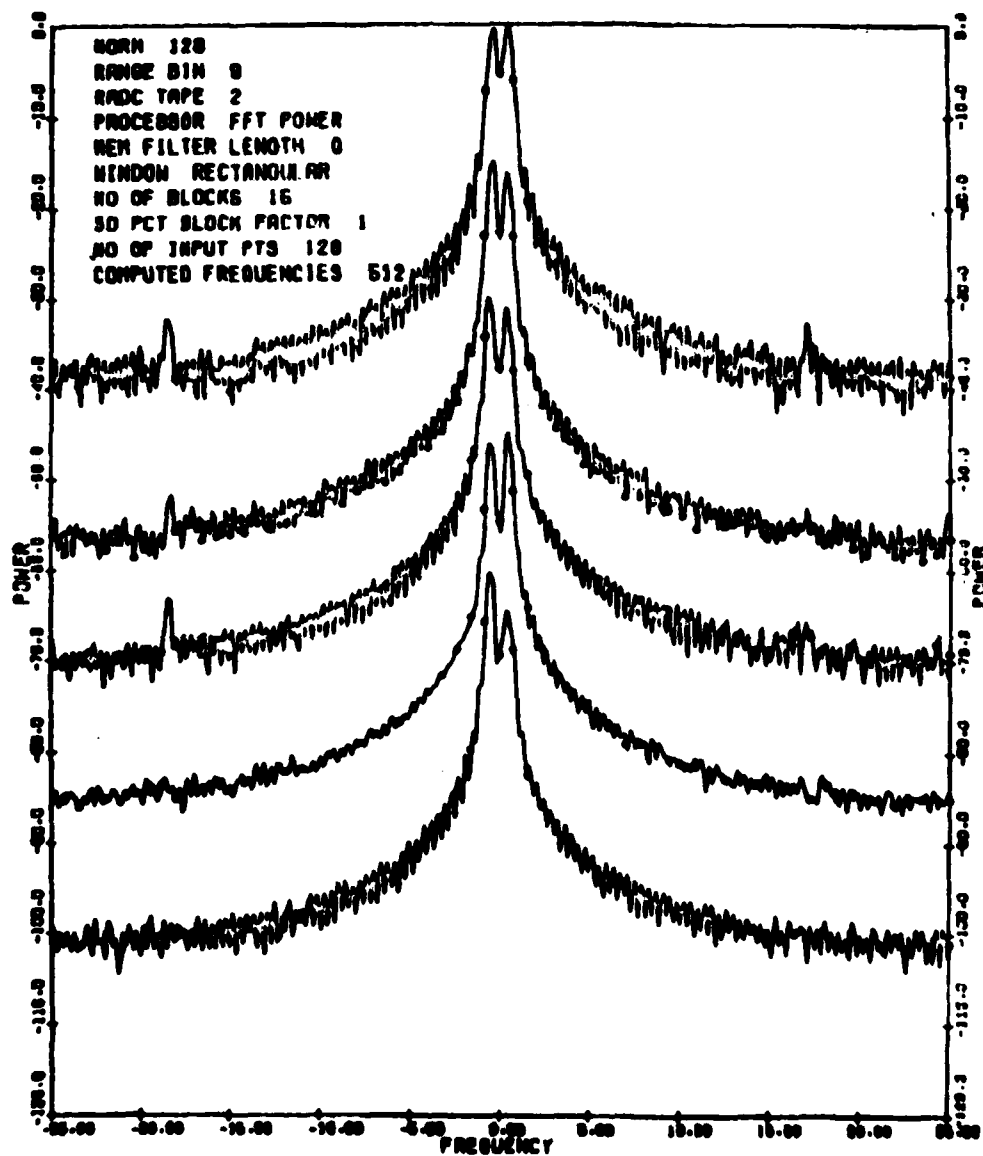


Figure 8. Sea Scatter, 128 Pt. Time Series (No Hanning) 512 Frequency FFT

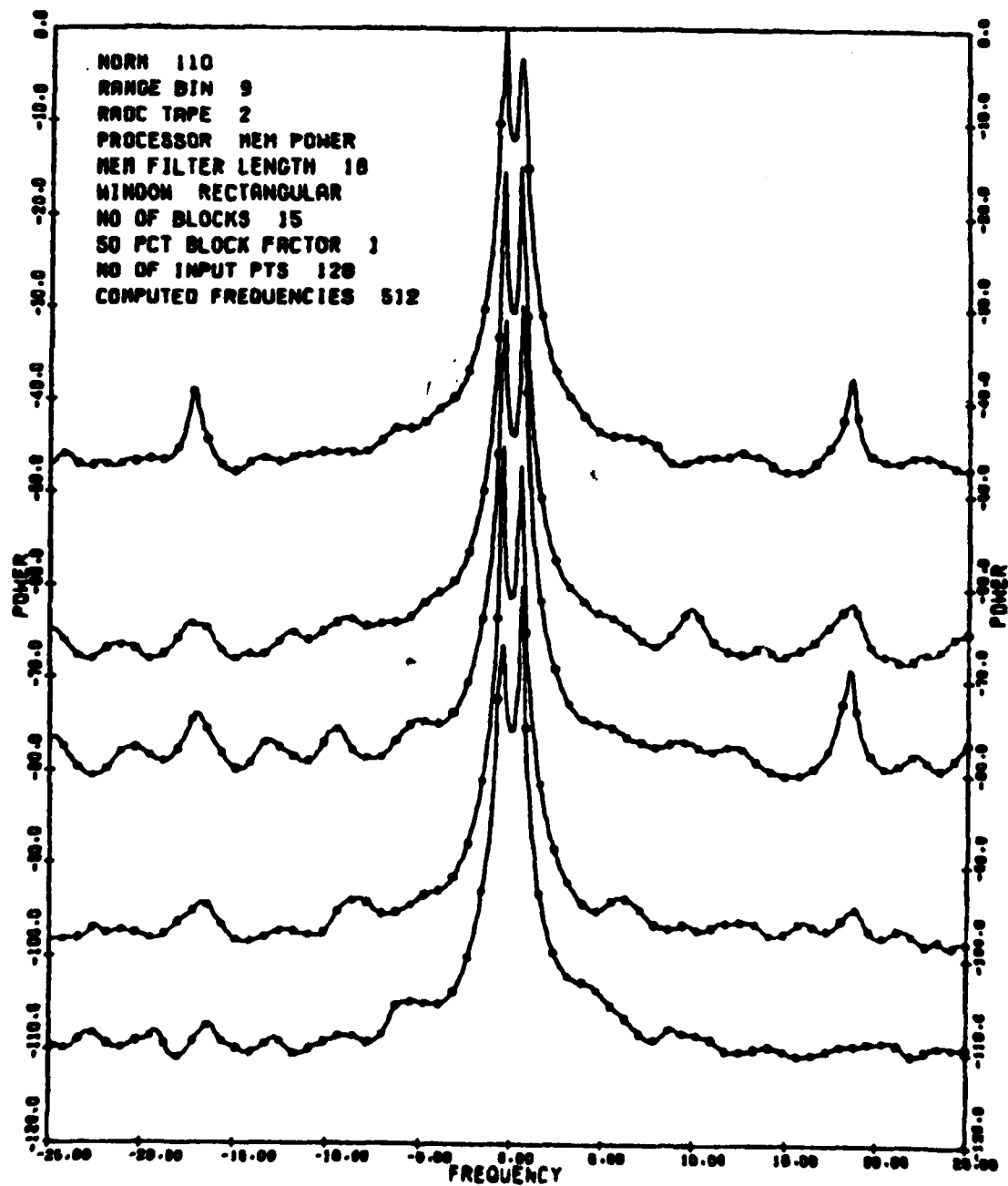


Figure 9. Sea Scatter, 128 Pt. Time Series, 16 Pole
MEM 512 Frequency DFT

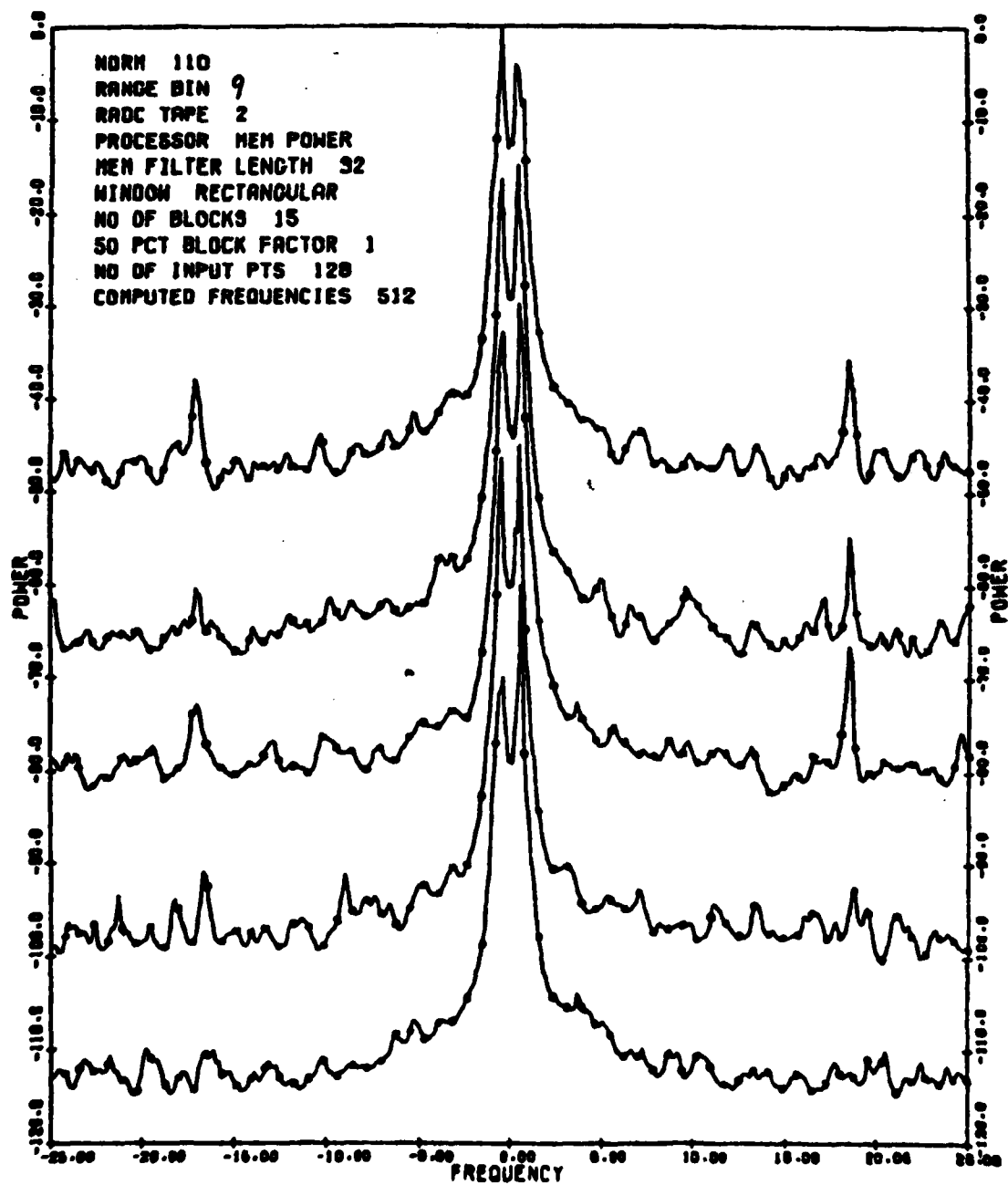


Figure 10. Sea Scatter, 128 Pt. Time Series, 32 Pole MEM
512 Frequency DFT

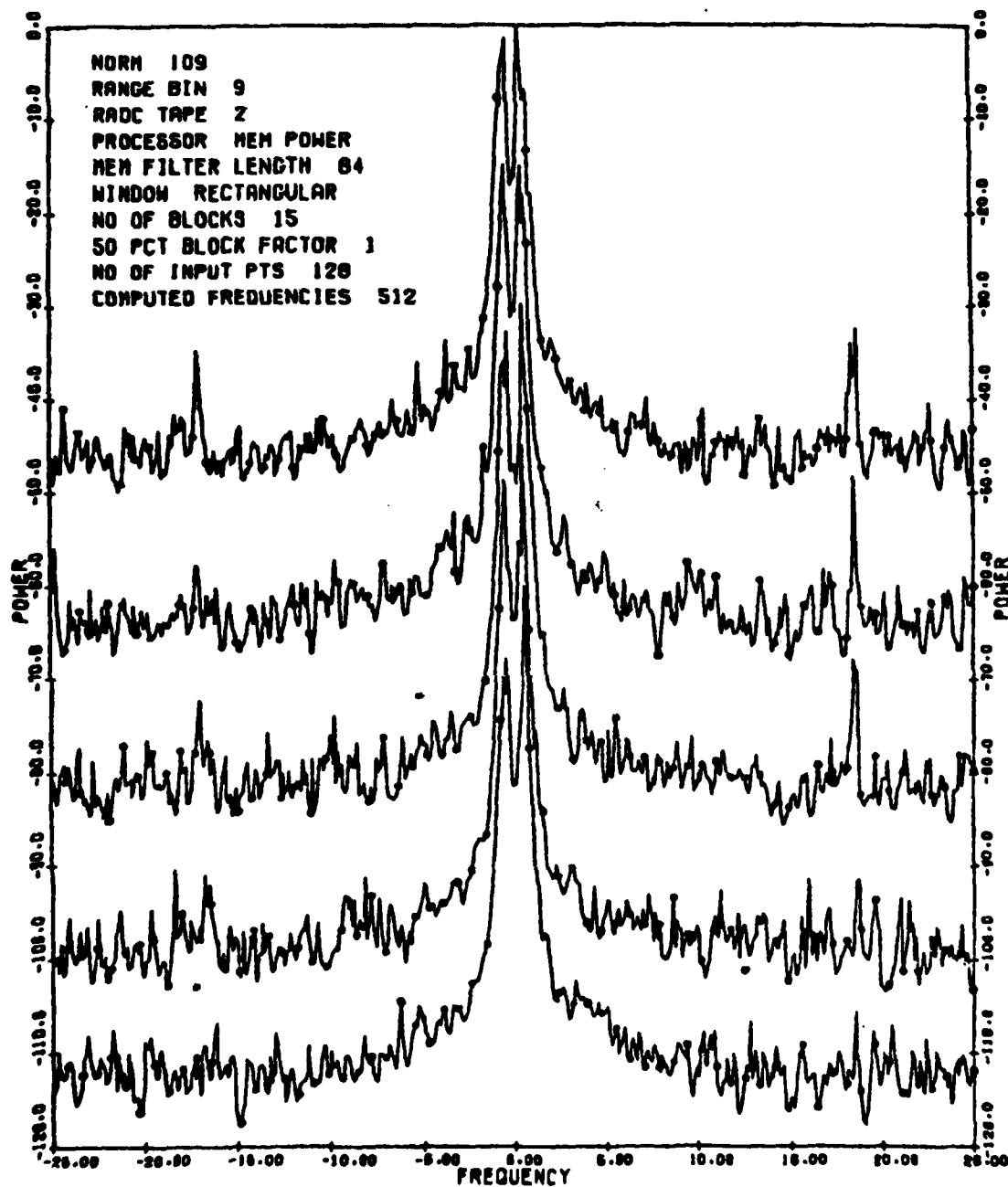


Figure 11. Sea Scatter, 128 Pt. Time Series, 64 Pole MEM
512 Frequency DFT

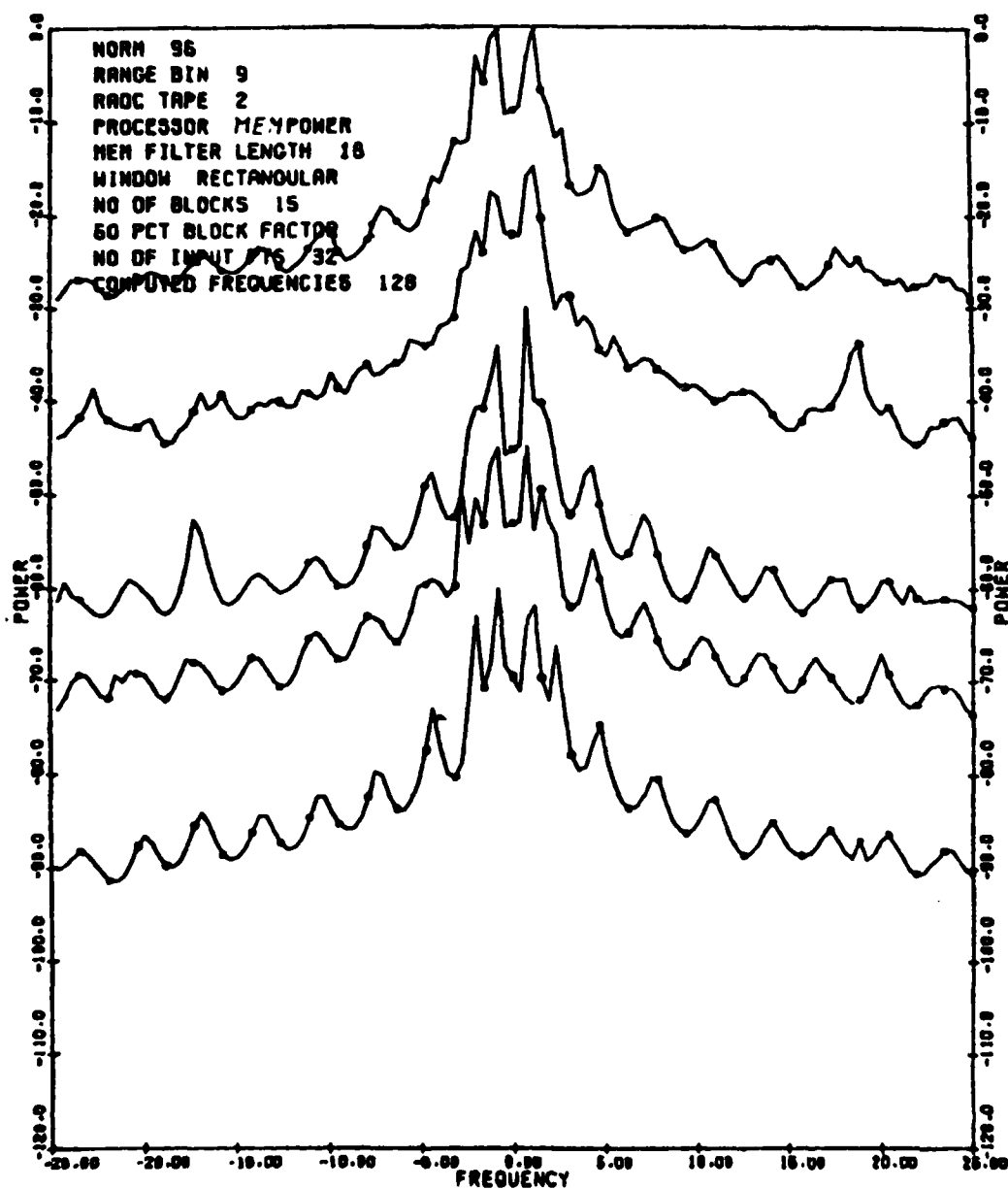


Figure 12. Sea Scatter, 32 Pt. Time Series, 16 Pole MEM
128 Frequency DFT

POLAR FOX II COVERAGE

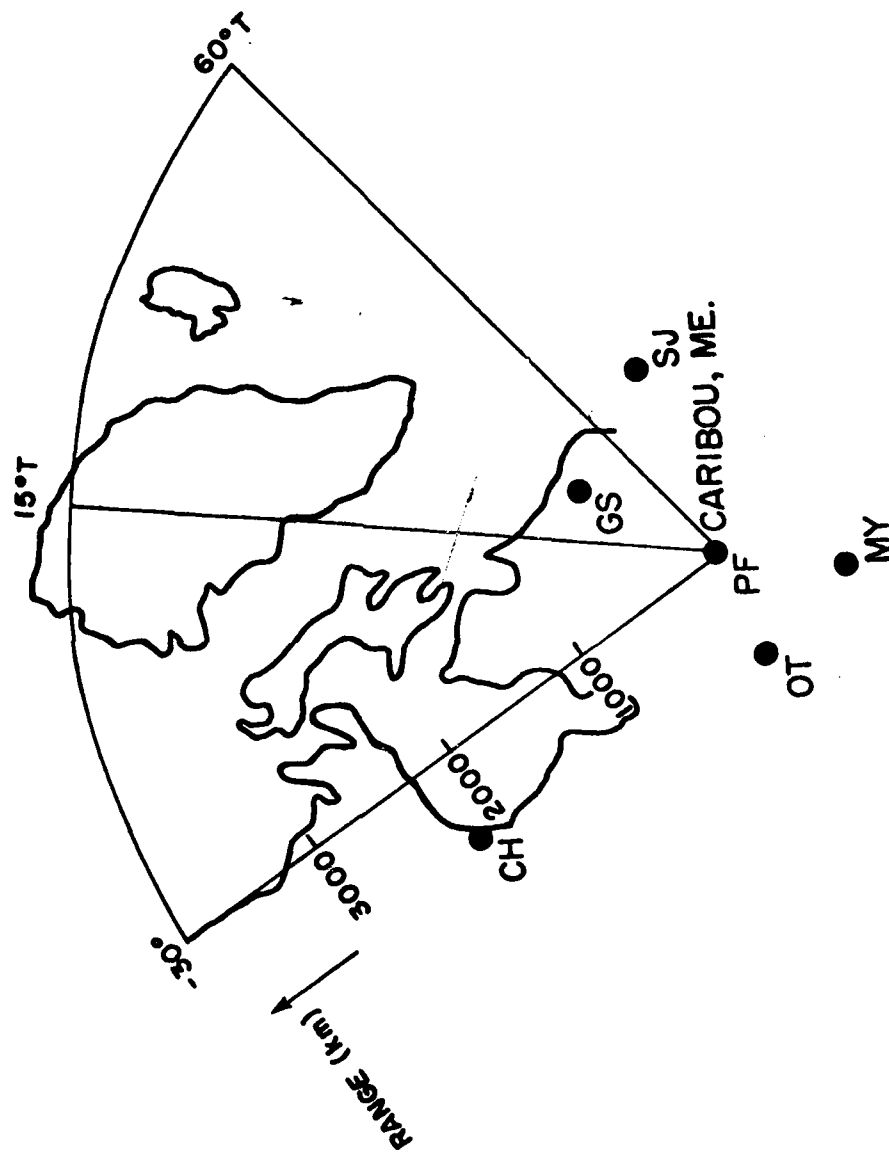
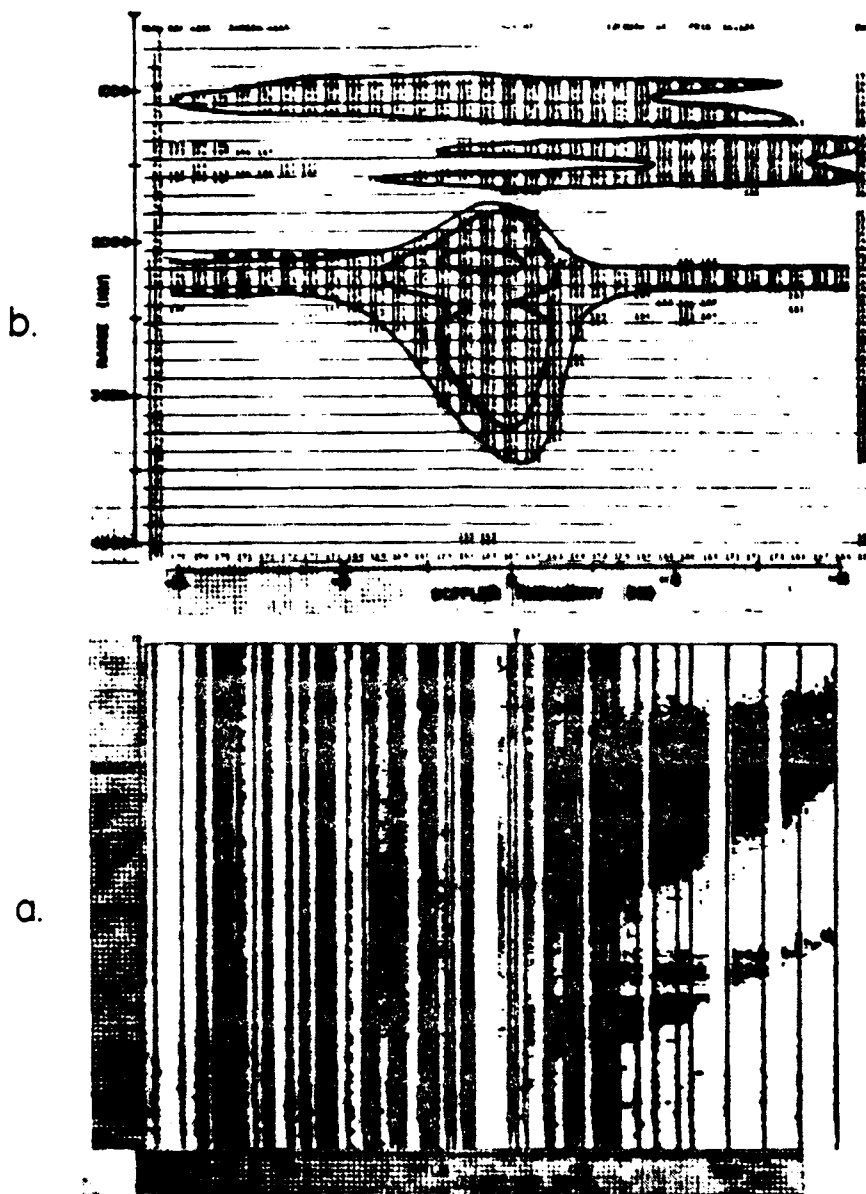


Figure 13. Polar Fox II Coverage



72/0325/18 UT
16.1 MHz

AZIMUTH = 40° T

Figure 14a. Signal Frequency vs. Range Ionogram
b. Doppler Frequency vs. Range B/S

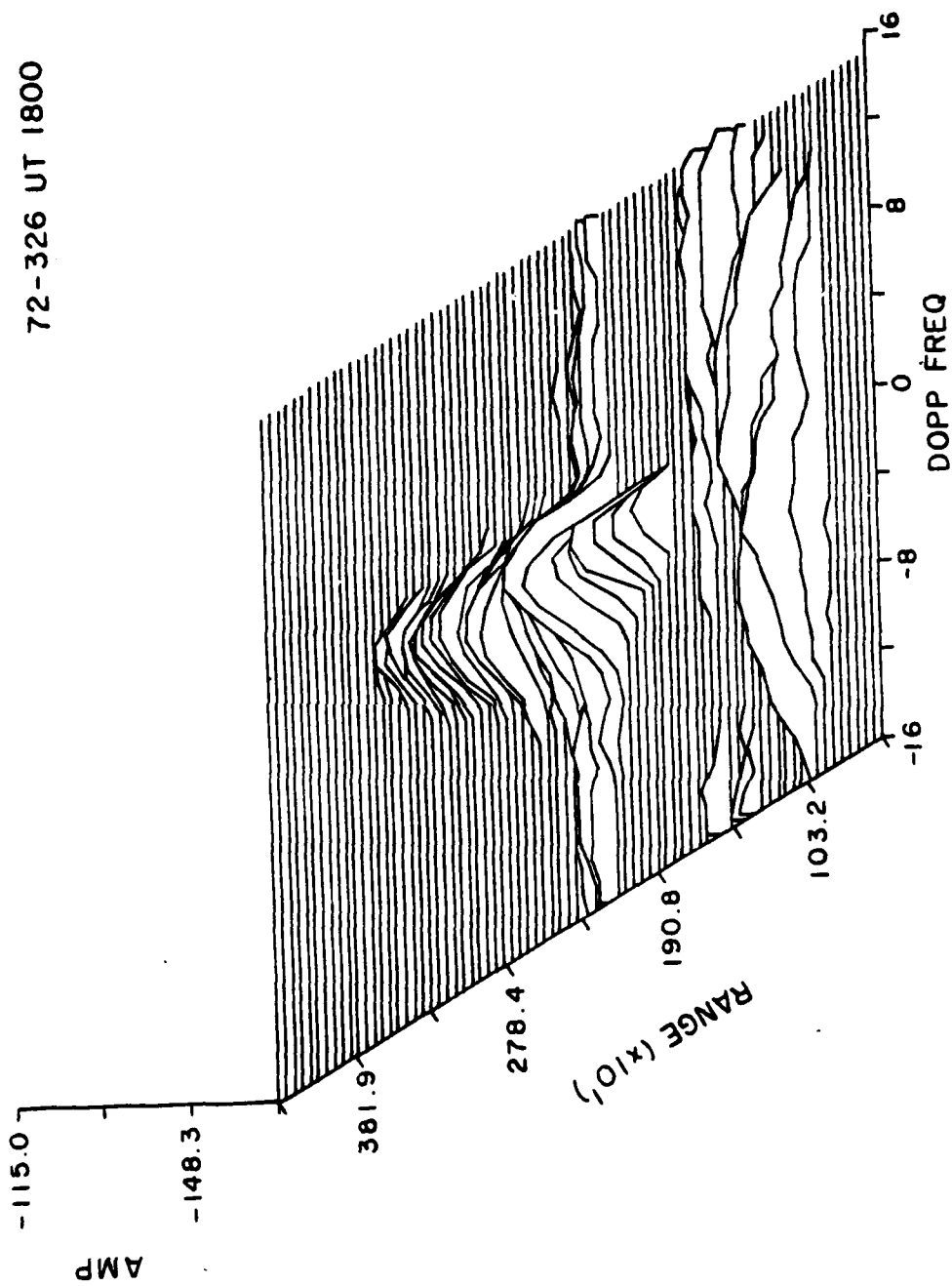
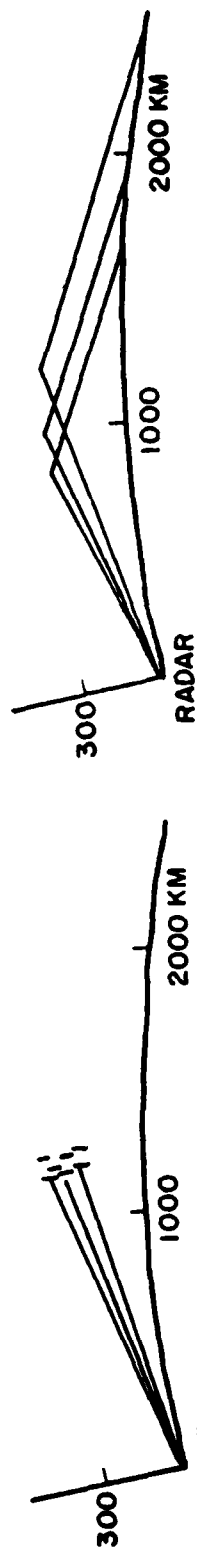


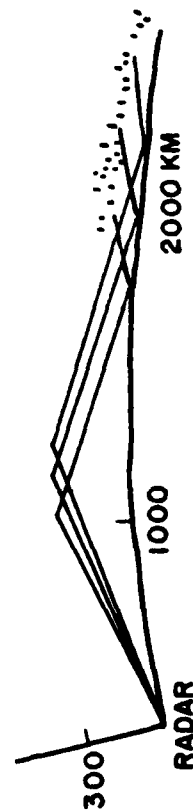
Figure 15. Three Dimensional Plot, Doppler vs. Range vs. Power

TYPES OF BACKSCATTER (B/S)



DIRECT IONOSPHERIC BACKSCATTER
(ONE LEG)

GROUND BACKSCATTER
(TWO LEG)



GROUND REFLECTION AND IONOSPHERIC BACKSCATTER
(THREE LEG)

Figure 16. Types of Backscatter (B/S)

EFFECTIVE VERTICAL ANGLE- θ (VOLUME SCATTERING)

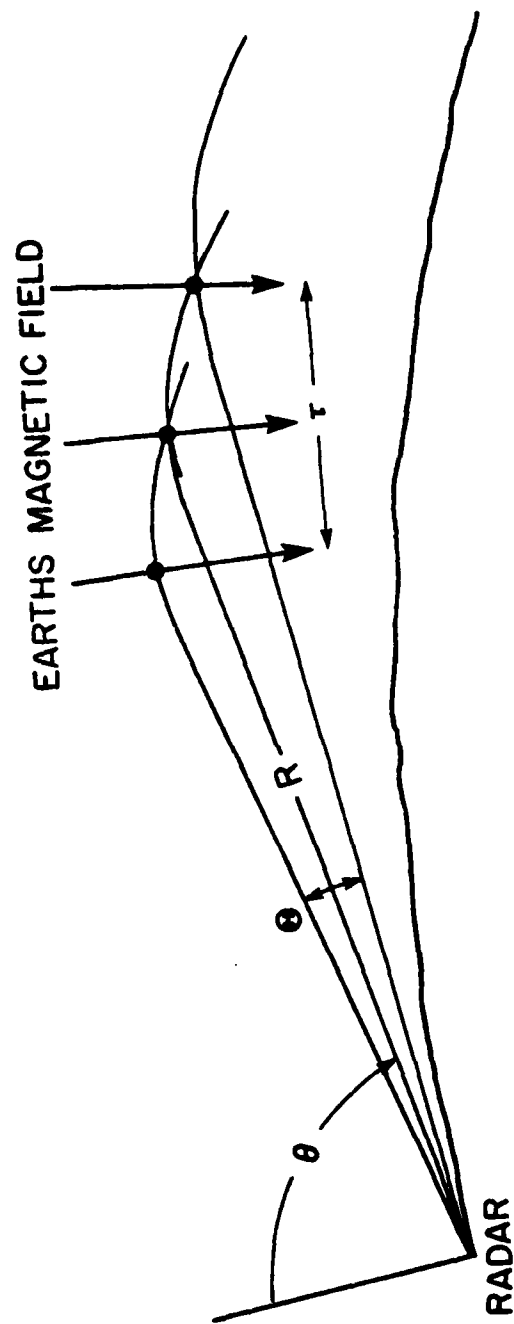


Figure 17. Effective Vertical Angle

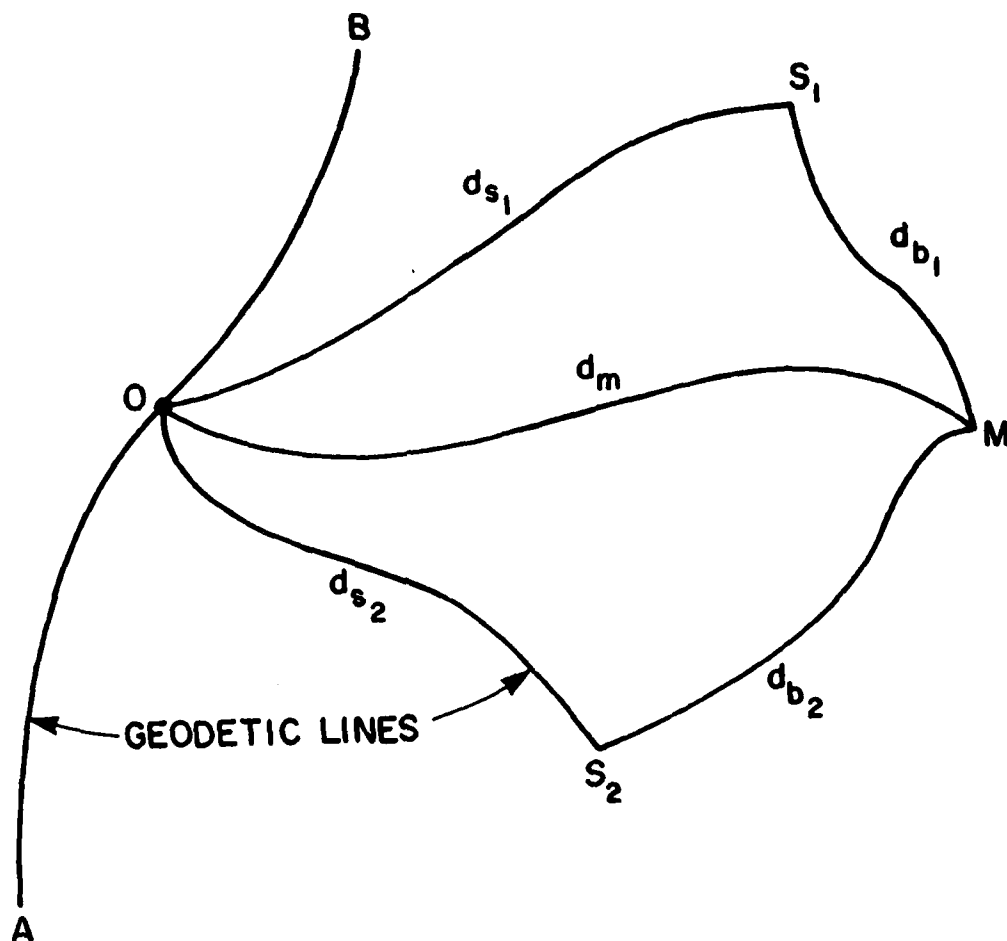


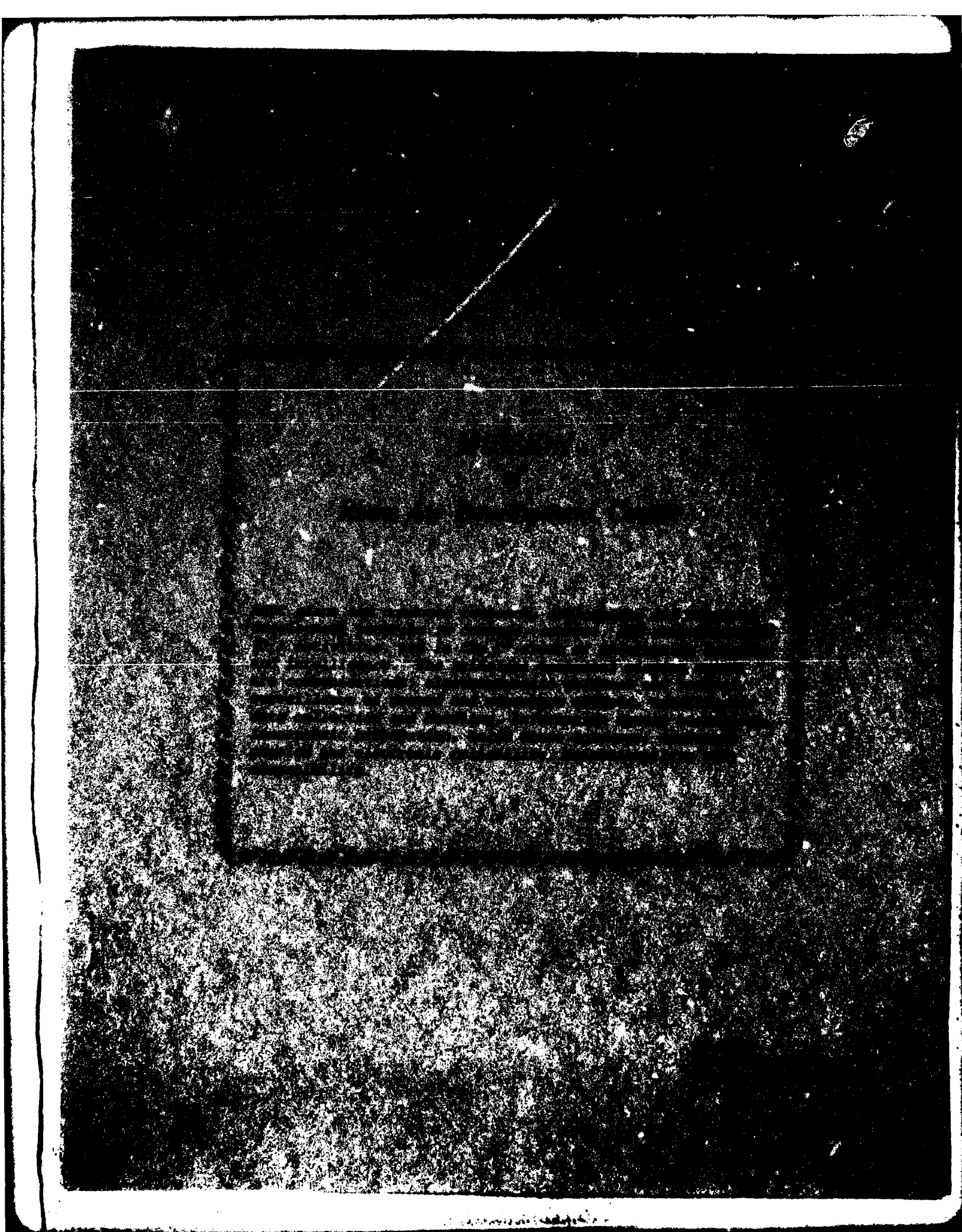
Figure 18. LORAN Navigation Hyperbolic Grid Radio Fix

REFERENCES

1. Lacoss, R. T., (1971), Geophysics 36:661.
2. Pfister, W., et al, Environmental Research Papers, N. 506, AFCRL-TR-75-0194.
3. Varad, R., et al (1975), "The Max.Likelihood Method Applications to DAASM Studies", Space Data Analysis Laboratory, Boston College, Final Report, AFCRL-TR-75-0551.
4. Burg, J. P. (1968), "A New Analysis Technique for Time Series", NATO Advanced Study Institute on Signal Processing, Enschede, Netherlands.
5. Smylie, D. E., Clarke, G. K. C. & Ulrych, T. J., Analysis of Irregularities in the Earth's Rotation in Methods in Computational Physics, Vol. 3, Academic Press, 1973.
6. Sales, G. S. (June 1977), "Ionospheric Backscatter Reflectivity", paper presented at the URSI Symposium, Stanford, Ca.
7. George, P. L. and Bradley, P. A., "A New Method of Predicting the Ionospheric Absorption of High Frequency Waves at Oblique Incidence", ITU Telecommunications Journal, Geneva, May, 1974.
8. Johler, J. R. & L. A. Berry (1967), LORAN-D Phase Report, IER59-ITSA56.
9. Johler, J. R. (1971), LORAN Radio Navigation Over Irregular, Inhomogeneous Ground with Effective Ground Impedance Maps, TRE Report, OT/TRER22.
10. Johler, J. R., D. C. Hyovalti & W. B. Jones, "Impedance Maps to Predict the Effect of Irregular, Inhomogeneous Ground on LORAN C/D Radio Navigation Systems", OT Report 73-6 (1973).

REFERENCES (Cont.)

11. Sodano, E. M. (1965), "General Non-Iterative Solution of the Inverse and Direct Geodetic Problem", Bulletin Geodeseque, No. 75, 69-89.
12. S. Horowitz (1977), "User's Guide to E.S.D. LORAN Grid Prediction Program", RADC-TR-77-407.
13. Cormier, R. J. and K. Dieter, "Automatic Processing of Digital Ionograms" (1974), AFCRL-TR-0502.
14. Cormier, R. J. and K. Dieter, "Radar Refraction Computations Using Digital Vertical-Incidence Ionograms" (1975), AFCRL-TR-75-0560.
15. Trizna, D. B. et al, "Directional Sea Spectrum Determination Using HF Doppler Radar Techniques (Jan. '77), IEEE Trans. AP-25, No. 1.
16. Sales, G. S., Videberg, J. I. & Varad, R. (1975), "DAASM Project-High Latitude HF Propagation Experiment", ERP No. 516, AFCRL-TR-75-0290.
17. Sales, G. S. and Videberg, J. I. (1976), "DAASM Project-High Latitude Aircraft HF Propagation Experiment, Part II", RADC-TR-76-235.
18. Martine, J. E. & Power, L. F., Jr. (1973), "Numerical and Data Analysis Techniques Applied to Scientific Research", AFCRL-TR-73-0433.
19. Nichols, B. E. (1973), "Propagation Measurements Program - (Polar Fox II): Antenna Patterns and Gains", PMP-6, Lincoln Lab.



DATE
FILMED
-8